N-Termini of *Eco*RI Restriction Endonuclease Dimer Are in Close Proximity on the Protein Surface†

Wei Liu,‡ Yu Chen,§ Heather Watrob,§ Sue G. Bartlett,‡ Linda Jen-Jacobson,|| and Mary D. Barkley*,§

Departments of Chemistry and Biochemistry, Louisiana State University, Baton Rouge, Louisiana 70803, Department of Chemistry, Case Western Reserve University, Cleveland, Ohio 44106, and Department of Biological Sciences, University of Pittsburgh, Pittsburgh, Pennsylvania 15260

Received March 11, 1998; Revised Manuscript Received August 20, 1998

ABSTRACT: The N-terminal region of *Eco*RI endonuclease is essential for cleavage yet is invisible in the 2.5 Å crystal structure of endonuclease−DNA complex [Kim, Y., Grable, J. C., Love, R., Greene, P. J., Rosenberg, J. M. (1990) *Science 249*, 1307−1309]. We used site-directed fluorescence spectroscopy and chemical cross-linking to locate the N-terminal region and assess its flexibility in the absence and presence of DNA substrate. The second amino acid in each subunit of the homodimer was replaced with cysteine and labeled with pyrene or reacted with bifunctional cross-linkers. The broad absorption spectra and characteristic excimer emission bands of pyrene-labeled muteins indicated stacking of the two pyrene rings in the homodimer. Proximity of N-terminal cysteines was confirmed by disulfide bond formation and chemical cross-linking. The dynamics of the N-terminal region were determined from time-resolved emission anisotropy measurements. The anisotropy decay had two components: a fast component with rotational correlation time of 0.3−3 ns representing probe internal motions and a slow component with 50−100 ns correlation time representing overall tumbling of the protein conjugate. We conclude that the N-termini are close together at the dimer interface with limited flexibility. Binding of Mg^{2+} cofactor or DNA substrate did not affect the location or flexibility of the N-terminal region as sensed by pyrene fluorescence and cross-linking, indicating that substrate binding is not accompanied by folding or unfolding of the N-terminus.

Type II restriction endonucleases are a large and important class of sequence-specific DNA enzymes with high selectivity (*1*, *2*). A few of the more than 2400 known restriction enzymes from a wide variety of prokaryotes (*3*) have been studied by biochemical and biophysical techniques. These enzymes are homodimers with no primary sequence homology, despite appreciable homology in the protein fold (*4*). *Eco*RI endonuclease recognizes the palindromic DNA sequence GAATTC to form a 2-fold symmetric complex (*5*−*7*). In the presence of Mg^{2+} cofactor, the enzyme cleaves DNA after G on each strand to produce 4-bp sticky ends. Energetic, crystallographic, and genetic analyses of *Eco*RI endonuclease have revealed fundamental concepts about the molecular basis of stringent discrimination. Energetic contributions due to direct and indirect readout of DNA sequence have been mapped along the entire protein−DNA interface (*8*). The X-ray structure of *Eco*RI endonuclease complexed with cognate DNA shows a highly redundant recognition network and identifies amino acid residues important for recognition and catalysis (*6*, *7*). Mutagenesis studies have confirmed the assignments of active-site residues as well as recognition residues (*9*−*13*). They also revealed additional residues outside of the protein−DNA interface that affect recognition and catalysis (*14*, *15*).

The N-termini of *Eco*RI endonuclease are essential for DNA cleavage. They also stabilize the *Eco*RI−DNA complex without affecting specificity (*16*). Proteolytic deletion of the first three residues of the polypeptide does not alter the rate of cleavage or the number of counterions released upon binding of cognate DNA. It has only a modest effect on the stability of the complex, with about 2-fold reduction in binding affinity and dissociation rate. Deletion of the first 11 residues, however, completely abolishes cleavage activity, reduces the number of counterions released by two, and destabilizes the complex about 60-fold. No further changes occur upon deletion of the first 28 residues. These deletion derivatives make the same DNA footprints, determined from ethylation interference patterns, and have the same sequence specificity, defined as the ratio of affinities for cognate and noncognate DNA, as intact endonuclease. The N-termini have been proposed to cooperate with the catalytic cleft in DNA cleavage.

The first 16 residues of the polypeptide chain are not resolved in the X-ray structure of the *Eco*RI−DNA complex (*6*). Several key questions about this critical region of *Eco*RI endonuclease are the following: Is the N-terminal region disordered and flexible or ordered in either the free enzyme or the DNA complex? Does the N-terminal region change conformation when the enzyme binds to DNA? How does

† This work was supported by NIH Grants GM29207 and GM35009.

* To whom correspondence should be addressed at the Department of Chemistry, Case Western Reserve University, 10900 Euclid Ave., Cleveland, OH 44106-7078. E-mail: mdb4@po.cwru.edu.

‡ Louisiana State University.

§ Case Western Reserve University.

|| University of Pittsburgh.

10.1021/bi980557f CCC: $15.00
Published on Web 10/16/1998

the N-terminal region promote DNA cleavage and stabilize the complex? In this paper we use site-directed fluorescence spectroscopy and chemical cross-linking to probe the proximity and mobility of the N-termini in *Eco*RI endonuclease. Pyrene fluorescent probes and chemical cross-linking reagents are reacted with a single cysteine in the N-terminal region of each subunit of the homodimer. Pyrene exhibits excimer fluorescence when the aromatic rings stack in parallel pairs about 3.5 Å apart (*17*).

EXPERIMENTAL PROCEDURES

Materials. *N*-(1-Pyrenyl)iodoacetamide and *N*-(1-pyrenyl)maleimide were purchased from Molecular Probes (Eugene, OR). 5,5′-Dithiobis(2-nitrobenzoate) and *N*-acetylcysteine were from Sigma (St. Louis, MO). 1,3-Phenyldimaleimide was from Aldrich (Milwaukee, WI). P-11 phosphocellulose was from Whatman (Hillsboro, OR). HTP hydroxyapatite and Bio-Rex 70 were from Bio-Rad (Hercules, CA). All other chemicals were the highest available grade. N,N'-$(CH_2)_n$bisiodoacetamide cross-linkers with $n =$ 2, 4, 7, 10, and 12 were synthesized and purified (*18*). Molecular weights were confirmed by fast atom bombardment mass spectrometry; purities of 86−99% were determined by ^{1}H NMR.

The 24-nt sequence d(GGGCGGGTGCGAATTCGCGGGCGG) and its complementary strand were synthesized by the Pittsburgh DNA Synthesis Facility and purified (*16*). The heteroduplex was annealed and end-labeled as described previously (*8*, *19*). The 13-nt sequence d(TCGCGAATTCGCG) was synthesized by Gene Lab in the Louisiana State University School of Veterinary Medicine and purified by reversed-phase HPLC (*20*) on a C18 column (300 Å pore size, 5 mm particle size) with a 50-min linear gradient of 15−20% buffer B. Buffer A was 0.1 M (triethylamino)-acetate, pH 7.0; buffer B was 0.1 M (triethylamino)acetate in 70% acetonitrile, pH 7.0. The 13-nt sequence was >98% pure as judged by denaturing PAGE.[1] The homoduplex was annealed by heating to 80 °C and cooling slowly to room temperature for 1 h.

NaCl buffer contains 10 mM sodium phosphate buffer, pH 7.0, NaCl at the indicated concentration, 1 mM EDTA, and 7 mM β-mercaptoethanol. Labeling buffer contains 20 mM sodium phosphate buffer, pH 7.0, NaCl at the indicated concentration, 10 mM EDTA, and 10% glycerol. Glass-distilled glycerol (EM Science, Cherry Hill, NJ) was used in buffers for optical experiments. Labeling buffer was purged with N_2 before use. Binding buffer contains 10 mM Bis-tris propane, pH 7.3, salt at the indicated concentration, 1 mM EDTA, 5 μM DTT, and 100 μg/mL bovine serum albumin. Solvent viscosity was measured at 4 °C in a Wells-Brookfield viscometer.

Site-Directed Mutagenesis. Site-directed mutagenesis was performed with the Altered Sites system from Promega (Madison, WI). The *Eco*RI genes were obtained from an expression vector pSCC2 carrying *Eco*RI endonuclease and methyltransferase genes under the control of a heat-inducible bacteriophage λ P_L promoter (*21*). The 241 bp upstream sequence between *Hin*dIII (0) and *Nde*I (241) in pSCC2 was deleted and a new *Nco*I (0) site was introduced, leaving a unique *Hin*dIII (1960) site in pSCC2 in the endonuclease gene. The gene fragment between *Mlu*I (1654) and *Hin*dIII (1960) for the first 67 residues of the N-terminal sequence of *Eco*RI endonuclease was cloned into pSELECT-1 vector, whose *Sma*I site had been changed into a *Mlu*I site. Mutagenesis was conducted with the double-stranded template protocol provided by the manufacturer. The oligonucleotide carrying the Ser2Cys mutation, d(TGG AAA CAT GGA TAC ATG TGT AAT AAA AAA CAG TCA), also carried a silent mutation to create a diagnostic *Afl*III restriction site (ACATGT) for screening mutants. Likewise, the sequence for the Asn3Cys mutation, d(GGA AAC ATG GAT ACA TGT CTT GTA AAA AAC AGT CAA ATA GGC), creates an *Afl*III restriction site. The *Mlu*I−*Hin*dIII insert carrying the newly created restriction site in pSELECT-1 was cloned back into the modified pSCC2 expression vector, which was then renamed pS2C or pN3C, referring to the Ser2Cys or Asn3Cys mutation. Mutations were confirmed by DNA sequencing of the inserts and by gas-phase protein sequencing of purified muteins. Amino acid sequence was determined at Baylor College of Medicine.

Protein Purification. Wild-type and mutant endonucleases were purified according to a published protocol (*22*) with several modifications. Transformed *E. coli* N4830 cells (Pharmacia; Uppsala, Sweden) were grown at 28 °C to an optical density of 1.0 at 600 nm. The temperature was raised to 42 °C to induce protein expression and cells were grown for 4 h. Cells were harvested by centrifugation at 10000*g* for 10 min at 4 °C. Cell paste (32 g) from 8 L of culture was sonicated in 200 mL of 0.4 M NaCl buffer, 0.1 mg/mL lysozyme, 10 mM protease inhibitor E-64, 1 mM leupeptin, and 200 mM phenylmethanesulfonyl fluoride. The cell lysate was centrifuged at 14700*g* for 1 h and the supernatant was loaded directly onto a 100-mL P-11 column (2.5 cm i.d.) equilibrated with 0.4 M NaCl buffer. The P-11 column was washed with 0.4 M NaCl buffer until the absorbance at 280 nm decreased to baseline, and the protein was eluted with a 500 mL salt gradient from 0.4 to 0.8 M NaCl. Endonuclease fractions were located by SDS−PAGE, pooled, and loaded directly onto a 30-mL HTP column (1.0 cm i.d.) equilibrated with 0.2 M NaCl buffer containing 10% glycerol without EDTA. The HTP column was washed with 0.2 M NaCl buffer containing 10% glycerol without EDTA and eluted with a 150 mL phosphate gradient from 0.01 to 0.5 M sodium phosphate. Endonuclease fractions were pooled, dialyzed overnight against 2 L of 0.4 M NaCl buffer containing 10% glycerol, and then loaded onto a 10-mL Bio-Rex 70 column (1.0 cm i.d.) equilibrated with 0.4 M NaCl buffer containing 10% glycerol. The Bio-Rex 70 column was washed with 0.4 M NaCl buffer containing 10% glycerol and eluted with a 60 mL salt gradient from 0.4 to 0.8 M NaCl. Purified *Eco*RI endonuclease (24 mg) was at least 99% pure as judged by SDS−PAGE. Protein concentration was determined by the Bio-Rad protein assay with an *Eco*RI endonuclease

[1] Abbreviations: Bis-tris propane, 1,3-bis[tris(hydroxymethyl)-methylamino]propane; 1,3-DM, 1,3-phenyldimaleimide; DMF, N,N'-dimethylformamide; DTNB, 5,5′-dithiobis(2-nitrobenzoate); DTT, dithiothreitol; EDTA, ethylenediaminetetraacetic acid; fwhm, full width at half-maximum; mutein, mutated protein; nMBI, N,N'-$(CH_2)_n$-bisiodoacetamide; PI, *N*-(1-pyrenyl)iodoacetamide; PI−Cys, conjugate of *N*-(1-pyrenyl)iodoacetamide and *N*-acetylcysteine; PI−N3C, conjugate of *N*-(1-pyrenyl)iodoacetamide and N3C mutein; PM, *N*-(1-pyrenyl)maleimide; PM-Cys, conjugate of *N*-(1-pyrenyl)maleimide and *N*-acetylcysteine; PM−N3C, conjugate of *N*-(1-pyrenyl)maleimide and N3C mutein; SDS, sodium dodecyl sulfate; PAGE, polyacrylamide gel electrophoresis.

standard solution, whose concentration had been determined by amino acid analysis. Molarity of endonuclease solutions was calculated assuming a dimer molecular mass of 62 kDa. Purified endonuclease was stored at −70 °C in 0.6 M NaCl buffer containing 10% glycerol. All experiments were performed at 4 °C except DNA binding and cleavage assays.

Fluorescent Labeling. Wild-type and mutant *Eco*RI endonucleases were dialyzed 4 × 4 h into 0.6 M NaCl labeling buffer to remove β-mercaptoethanol. To label both N-termini, a 2.4-fold molar excess of freshly prepared PI or PM in cold DMF (1.0 mg/mL) was added to 0.5 mL of 1×10^{-5} M endonuclease. The volume of DMF added was <10%. The reaction mixture was kept on ice in the dark. The labeling reaction was terminated after 2 h for PM and after 10 h for PI by reaction with 5 μL of 0.1 M DTT for 2 h. Labeled endonuclease was dialyzed into 0.6 M NaCl buffer containing 10% glycerol without β-mercaptoethanol. The extent of labeling was estimated by absorbance, using extinction coefficients of 2.8×10^4 M^{-1} cm^{-1} at 344 nm for PI and 3.6×10^4 M^{-1} cm^{-1} at 339 nm for PM (*23*). Stoichiometric labeling of the N3C mutein was achieved with molar ratios of pyrene:N3C between 1.96 and 2.0. To label only one N-terminus, the PI labeling reaction was terminated after 15 min. Alternatively, a 0.05 molar ratio of PI:N3C was used and the reaction was terminated after 100 h.

N-Acetylcysteine conjugates were made by reacting PI and PM with a 5-fold molar excess of *N*-acetylcysteine in methanol at room temperature in the dark for 24 h. The product was purified by flash chromatography on a silica column. Purified conjugate migrated as a single spot on TLC developed with *n*-butanol−H_2O−CH_3COOH (4:4:2).

The following NaCl buffers containing 10% glycerol without β-mercaptoethanol were used for optical experiments: endonuclease and *N*-acetylcysteine conjugates, 0.6 M NaCl; *Eco*RI−DNA complex, 0.1 M NaCl; *Eco*RI−Mg^{2+} complex, 0.6 M NaCl, and 20 mM $MgCl_2$.

Chemical Cross-Linking. Wild-type and N3C mutant *Eco*RI endonucleases were dialyzed 4 × 4 h into labeling buffer. Equimolar amounts of cross-linking reagent in cold DMF (0.125 mg/mL) were added to 100 μL of the following solutions and mixed rapidly: 1.6×10^{-6} M endonuclease in 0.6 M NaCl labeling buffer; 1.6×10^{-6} M *Eco*RI−DNA complex in 0.1 M NaCl labeling buffer; and 1.6×10^{-6} M *Eco*RI−Mg^{2+} complex in 0.6 M NaCl labeling buffer containing 20 mM $MgCl_2$. The volume of DMF added was <10%. Cross-linking reaction mixtures were incubated on ice in the dark for 10 h, terminated by reaction with 1 μL of 0.1 M DTT for 2 h, denatured by heating with 2.5% SDS, and analyzed by SDS−PAGE. DTT was not added to samples cross-linked with DTNB. Consequently, a small amount (<10%) of higher aggregates was observed due to intermolecular cross-linking of cross-linked dimer after SDS denaturation. We also noted higher aggregates of endonuclease in cross-linked samples that had been stored for 2 or more days at 4 °C. Higher aggregates may involve Cys218 in denatured samples or other slowly reacting functional groups on the surface of native samples. The degree of cross-linking was determined from digitized SDS−PAGE gel pictures using the ImageQuant software from Molecular Dynamics (Sunnyvale, CA).

DNA Binding and Cleavage. Endonuclease and 24-nt substrate d(GGGCGGGTGCGAATTCGCGGGCGG) were mixed in binding buffer. Equilibrium association constants K_A and dissociation rate constants k_d were determined by membrane filtration using the method of Riggs et al. (*24*, *25*) as modified by Jen-Jacobson et al. (*16*, *26*). Reaction mixtures were equilibrated for 30 min at 22 °C. First-order cleavage rate constants k_{cleave} were determined as described elsewhere (*8*, *19*). The heteroduplex substrate carries the GAATTC site off-center, so that cleavage in each of the DNA strands gives rise to a distinguishable product.

Absorption and Steady-State Fluorescence. Absorption spectra were recorded on an Aviv 118DS spectrophotometer. Fluorescence emission was measured in the ratio mode on a SLM 8000C photon counting spectrofluorometer. Sample absorbance at 340 nm was <0.1 with 3-mm path length. Excitation and emission monochromators were set at 4-nm band-pass. Emission spectra were collected with excitation polarizer at 54.7° and emission polarizer at 0° to the vertical, and background fluorescence from a solvent blank was subtracted. (Background fluorescence of buffer and unlabeled protein was the same.) Spectra were corrected by correction factors determined with a standard lamp from Optronics. Temperature was controlled at 4 °C by a circulating water bath. The sample compartment was purged with nitrogen gas to prevent condensation.

Steady-state emission anisotropy was measured in the L format. Fundamental anisotropy r_0 was measured in a transparent glass sample at 77 K using an Oxford Instruments variable-temperature liquid nitrogen cryostat DN1704 in the sample chamber of the SLM. The solvent was 0.6 M NaCl buffer containing 50% glycerol without β-mercaptoethanol. The emission anisotropy r is given by

$$r = (I_{VV} - GI_{VH})/(I_{VV} + 2GI_{VH}) \quad (1)$$

where the first and second subscripts refer to orientation of the excitation and emission polarizers, respectively. V is vertical (0°), H is horizontal (90°), and $G = I_{HV}/I_{HH}$ is a correction factor for the polarization dependence of the emission train.

Time-Resolved Fluorescence. Fluorescence decays were measured by time-correlated single photon counting. The excitation source was a Coherent 701 DCM dye laser pumped with an Antares 76-S mode-locked Nd−YAG laser. The output beam from the dye laser was passed through a BBO crystal to frequency-double into the UV followed by two 1-mm UG-11 filters (Schott) to remove the fundamental. Excitation wavelength was 320 nm. Emission wavelength (8-nm band-pass) was selected by an Instruments SA H-10 monochromator. The incident light was vertically polarized. The emission polarizer was set at 55° to the vertical for lifetime experiments. A DPU-2.5 optical depolarizer (Optics for Research) was placed before the emission monochromator for anisotropy experiments to eliminate polarization dependence of the detection train, so that $G = 1$. The instrument response function was 100 ps fwhm.

Fluorescence decay data were acquired contemporaneously from a fluorescent sample, solvent blank, and solution of coffee creamer in water for the instrument response. Temperature was controlled at 4 °C by a circulating water bath. The sample compartment was purged with nitrogen gas to prevent condensation. Data were collected in 1024 channels of 10−80 ps/channel. Solvent blank was subtracted and

sample decay data were deconvolved using the Beechem global program (*27*). Quality of fit is judged by reduced χ_r^2, weighted residuals, and autocorrelation function of the weighted residuals.

Fluorescence intensity decay $I(t)$ was fit to a sum of exponentials

$$I(t) = \sum \alpha_i \exp(-t/\tau_i) \quad (2)$$

with amplitude α_i and lifetime τ_i. Time-resolved emission spectral data were deconvolved using the Beechem global program (*27*). Decay-associated spectra $F_i(\lambda)$ of the ith component were calculated by combining the steady-state emission spectrum $F(\lambda)$ and time-resolved data:

$$F_i(\lambda) = \alpha_i(\lambda)\tau_i F(\lambda)/\sum \alpha_i(\lambda)\tau_i \quad (3)$$

Fluorescence anisotropy decay $r(t)$ of an anisotropic rigid molecule is a sum of five exponential terms:

$$r(t) = \sum \beta_i \exp(-t/\phi_i) \quad (4)$$

with preexponential β_i and rotational correlation time ϕ_i. The initial anisotropy $r(0) = \sum \beta_i$. For globular proteins the rotational correlation time can be estimated by the Stokes−Einstein equation:

$$\phi = \eta M(\bar{v} + h)/RT \quad (5)$$

where η is solvent viscosity, M is molecular weight, $\bar{v}$ is specific volume (typically 0.73 mL/g), h is hydration (typically 0.2 g of H_2O/g of protein), R is the gas constant, and T is absolute temperature. Individual polarized decays $I_{VV}(t)$ and $I_{VH}(t)$ are deconvolved simultaneously with a magic angle decay $I(t)$ in the Beechem global program:

$$I_{VV}(t) = I(t)[1 + 2r(t)]/3 \quad (6a)$$

$$I_{VH}(t) = GI(t)[1 - r(t)]/3 \quad (6b)$$

RESULTS

Mutant Endonucleases. Wild-type and mutant endonucleases were purified to homogeneity. Yields were about 0.75 mg of protein/g of cells for wild-type, S2C mutein, and N3C mutein. The purification procedure was streamlined by lysing the cells in a smaller volume of buffer with lysozyme and by loading and washing the phosphocellulose and Bio-Rex 70 columns with 0.4 M instead of 0.2 M NaCl buffer (*22*). Both wild-type and mutant endonucleases eluted from the columns at the expected salt concentrations (0.6 M NaCl for phosphocellulose and Bio-Rex 70, 0.2 M phosphate for hydroxyapatite) and cleaved λ DNA into the same restriction fragments on agarose gels (not shown). It is important to note that the functional form of *Eco*RI endonuclease is a dimer (*26*, *28*). In the absence of DNA, endonuclease aggregates to higher oligomers at salt concentrations <0.15 M NaCl and protein concentrations $>1 \times 10^{-7}$ M. No detectable dissociation into monomers occurs at protein concentrations $\geq 1 \times 10^{-11}$ M at any salt concentration (*28*; M. Kurpiewski and L. Jen-Jacobson, unpublished results). All experiments reported here were carried out under conditions of salt concentration, protein concentration, and temperature in which *Eco*RI endonuclease has been verified by gel filtration to be almost exclusively in the dimer form in the absence and presence of cognate DNA (*16*, *26*).

Table 1: DNA Binding Data[a]

endonuclease	K_A[b] (10^{10} M^{-1})	k_d[c] (10^{-5} s^{-1})	k_{cleave}[d] (s^{-1})
wild type	7.5 ± 0.3	4.8	0.45 ± 0.1
N3C	7.6 ± 0.5	3.6	nd
PI−N3C	6.4 ± 0.5	nd	nd
PM−N3C	4.4 ± 0.9	6.0	0.47 ± 0.3

[a] DNA substrate for binding and cleavage was GGGCGGGTGC-GAATTCGCGGGCGG. Errors are standard deviations from at least 5 experiments. [b] In 0.16 M NaCl, 22 °C. [c] In 0.1 M NaCl, 22 °C. [d] In 0.1 M NaCl and 12 mM Mg^{2+}, 22 °C. Single-turnover cleavage rates of top and bottom strands were identical within error limits. [e] nd, not determined.

The absorption spectra of the muteins is the same as that of wild-type with a maximum at 278 nm (*28*). N3C mutein reacted readily with iodoacetamide and maleimide pyrene labels, PI and PM. The labeling reaction is much faster for maleimide than iodoacetamide, as determined by RP-HPLC monitoring both absorbance at 280 nm and fluorescence at 330 nm excitation wavelength, 400 nm emission wavelength. Stoichiometric labeling of N3C mutein was achieved with a slight excess of label. However, wild-type and S2C mutein were not labeled even after 10 h of incubation. N-Terminal sequencing of S2C mutein gave an unidentified peak for the first residue, which eluted near tryptophan. Evidently, the terminal cysteine in S2C underwent a posttranslational modification that blocks the sulfhydryl group. A similar in vivo modification of N-terminal cysteine was reported for a carbonic anhydrase isozyme isolated from *Chlamydomonas* (*29*).

DNA Binding and Cleavage. Wild-type and N3C endonucleases bind to cognate 24 bp oligomer with identical association constants (Table 1). Fluorescent labeling of N3C lowers the binding affinity only slightly. Dissociation rates of N3C−DNA and PM−N3C−DNA complexes likewise differ little from the wild-type value. Moreover, the first-order rate constants for cleavage of both strands of the 24 bp substrate are identical for wild-type and PM-N3C endonucleases. These data indicate that neither the cysteine substitution nor the bulky fluorescent probe perturbs recognition or catalysis to any significant extent.

Absorption and Steady-State Fluorescence Spectra. The pyrene absorption spectra for PI- and PM-labeled N3C mutein as well as the respective *N*-acetylcysteine conjugates are shown in Figure 1. All spectra have typical pyrene absorption bands at about 325 and 345 nm. The spectra are broader and red-shifted in the protein conjugates compared to the cysteine conjugates. The fluorescence emission spectra of PI−N3C and PM−N3C excited at 340 nm have the structured pyrene monomer band around 400 nm. However, PI−N3C also has a large, unstructured, red-shifted band at 480 nm characteristic of excimer emission (Figure 2). PM−N3C has much less excimer emission, but the excimer band is obvious after subtraction of the small contribution from monomer emission in the excimer region of the spectrum (not shown). The intensity ratios of excimer to monomer emission are independent of protein concentration from 0.5 to 15 μM in both PI−N3C (inset of Figure 2) and PM−N3C, consistent with an intramolecular excimer. The

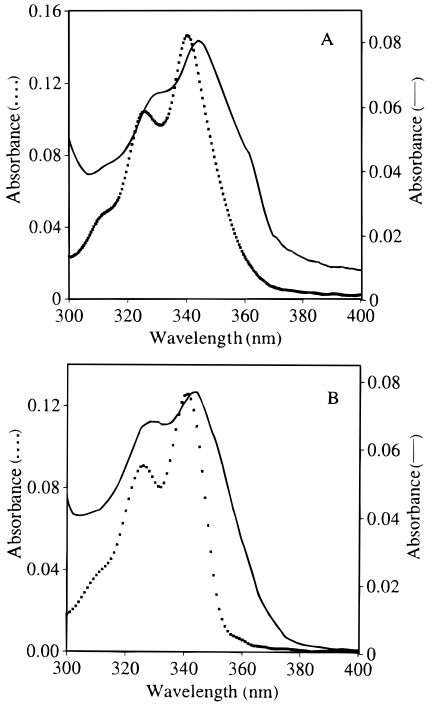

FIGURE 1: Absorption spectra of pyrene-labeled N3C muteins. (—) Labeled N3C; (···) labeled *N*-acetylcysteine. (A) PI conjugates; (B) PM conjugates.

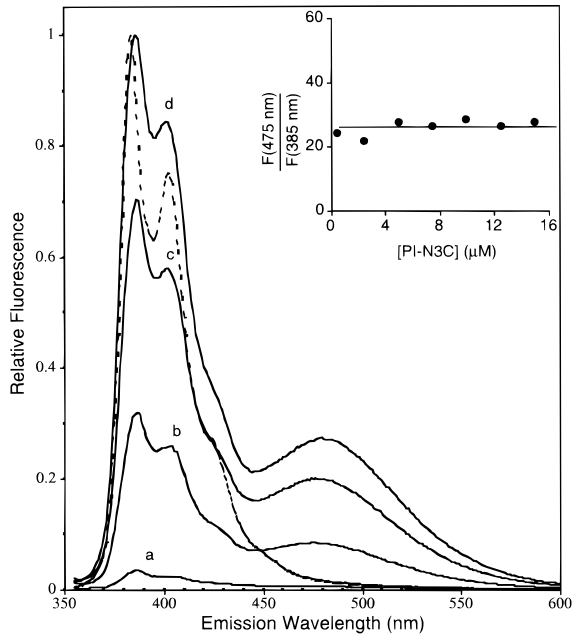

FIGURE 2: Concentration dependence of steady-state fluorescence emission spectra of PI−N3C at 340 nm excitation wavelength. (—) (a) 0.5, (b) 5, (c) 10, and (d) 15 μM; (- - -) PI−Cys. Inset plots the intensity ratio of excimer (475 nm) to monomer (385 nm) emission as a function of PI−N3C concentration.

presence of an intramolecular pyrene excimer in *Eco*RI endonuclease indicates close proximity of the two N-termini in the homodimer. S−S distances calculated by molecular modeling for excimers with fully overlapped pyrenes are 11 Å with the iodoacetamide linker and 17 Å with the maleimide linker.

The fluorescence emission and excitation spectra of pyrene-labeled N3C mutein depend on excitation and emission wavelength, respectively, whereas the fluorescence

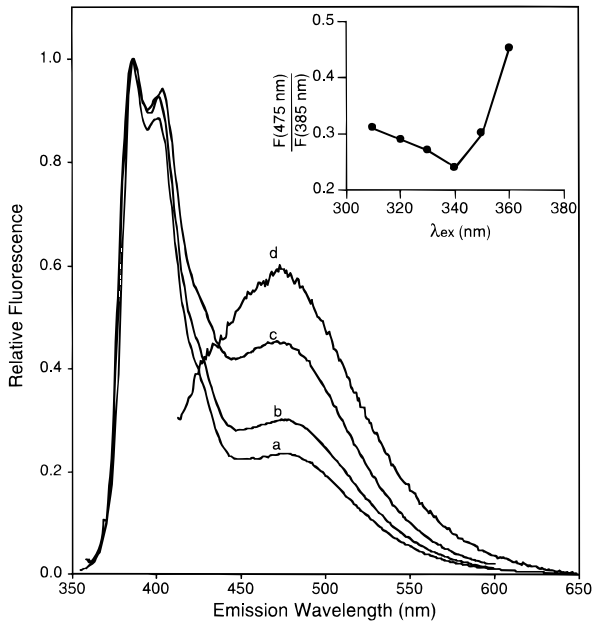

FIGURE 3: Excitation wavelength dependence of fluorescence emission spectra of PI−N3C: (a) 340, (b) 350, (c) 360, and (d) 400 nm. Inset plots the intensity ratio of excimer (475 nm) to monomer (385 nm) emission as a function of excitation wavelength.

spectra of cysteine conjugate are wavelength-independent. When PI−N3C is excited at 340 nm, both monomer and excimer emission are observed (Figure 3). The intensity ratio varies with excitation wavelength, increasing slightly to the blue and sharply to the red of the minimum at 340 nm (inset of Figure 3). Excitation spectra monitored on either side of the monomer band at 375 and 420 nm have similar shapes with maxima at about 345 nm (not shown). The excitation spectrum monitored in the excimer band at 485 nm is broader with maximum at 350 nm and a bulge at longer wavelength like the absorption spectrum. The wavelength dependence of the fluorescence spectra as well as the broadened and red-shifted absorption spectra indicate a heterogeneous ground-state environment of the pyrene chromophore in the protein conjugates. Because of hydrophobic interactions in aqueous solution, two pyrene rings joined by a short tether have stacked ground-state configurations (*30*). These stacked configurations are generally different from the excimer configuration. If the tether is flexible, excited stacked pyrenes can reorient to the excimer configuration with characteristic excimer emission. Lehrer (*31*) has proposed that solvent-exposed pyrenes attached to proteins will stack unless restrained by the protein, so that the monomer and excimer emission of protein-bound pyrenes would represent different stacked configurations. This interpretation suggests three fluorescent species of pyrene on N3C mutein: unstacked, stacked, and excimer. Stacked pyrenes including excimer configurations account for the red-shifted absorption spectra and the increase in the intensity ratio of excimer to monomer emission above 340 nm excitation wavelength. Unstacked pyrene is suggested by the different excitation spectra of monomer and excimer emission bands, assuming that the two emission bands would have similar excitation spectra if both derived from pyrene stacks.

Substrate or cofactor binding apparently has no effect on the intensity ratios of excimer to monomer emission in either PI−N3C or PM−N3C. The emission spectra of 2.7 μM

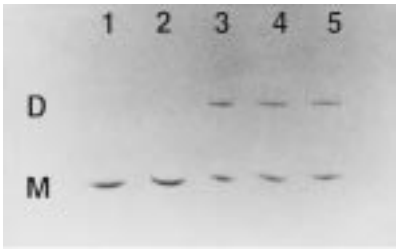

FIGURE 4: SDS−PAGE of cross-linking reaction mixtures of wild-type endonuclease and N3C mutein. Lanes contain the following: (1) wild type + 2MBI, (2) N3C, (3) N3C + DTNB, (4) N3C + 1,3-DMI, and (5) N3C + 2MBI. Monomer (M) and dimer (D) bands are also indicated.

Table 2: Cross-linking of Cys3 Residues

reagent	% cross-linking N3C	N3C + DNA	N3C + Mg^{2+}	S−S distance[a] (Å)
DTNB	46	50	55	2.5
1,3-DMI	63			10
2MBI	37	31	30	11
4MBI	34	33	34	12
7MBI	35	32	37	14
10MBI	9	11	5	19
12MBI	0	0	0	21

[a] Maximum distance between sulfur atoms in dicysteine conjugate calculated by molecular modeling.

*Eco*RI−DNA complexes of PI−N3C and PM−N3C with 13-mer cognate DNA duplex were identical to the spectra of 2.7 μM pyrene-labeled N3C mutein alone. Likewise the emission spectra of 15 μM PI−N3C and PM−N3C were the same in the Mg^{2+} complex and the free enzyme. Neither cognate DNA nor Mg^{2+} affected the concentration independence of the intensity ratio or the wavelength dependence of the excitation and emission spectra. These results indicate that substrate and cofactor binding do not alter the proximity of the two pyrenes in the respective enzyme complexes.

Cysteine Cross-Linking. The proximity of the N-termini of N3C mutant endonuclease was confirmed by chemical cross-linking of the two subunits using three bifunctional sulfhydryl reagents: DTNB, 1,3-phenyldimaleimide, and 2MBI. DTNB promotes disulfide bond formation through sulfhydryl−disulfide exchange reactions, whereas DMI and 2MBI react with cysteine sulfhydryl groups through maleimide and iodoacetamide functional groups. Covalently cross-linked dimers were formed in N3C mutein as shown by SDS−PAGE analysis (Figure 4). Wild-type enzyme could not be cross-linked, even though *Eco*RI endonuclease has a cysteine at position 218. Thus, intramolecular cross-linking occurred at Cys3 and not at the unreactive Cys218. This is consistent with the fact that wild-type endonuclease could not be labeled by sulfhydryl reagents. Under most conditions, no apparent higher oligomers were observed resulting from cross-links between Cys218 or other residues of cross-linked N3C dimers (see Experimental Procedures). The cross-linking data suggest a distance between the two Cys3 residues in the homodimer as short as 2.5 Å, the disulfide bond length. Increasing the spacer length did not increase the cross-linking yield, which remained constant in a series of *n*MBI bridging reagents for $n = 2$, 4, and 7 (Table 2). Reichert et al. (*32*) observed cross-linking yields that were independent of length for intermediate-size spacers between thiols of close proximity in actin−thymosin β4 complex. The large drop in cross-linking yield for $n = 10$ as well as weak excimer fluorescence in PM−N3C point to a maximum possible interthiol distance in N3C of 18 Å. Binding of cognate DNA or Mg^{2+} does not affect the extent of cross-linking, in agreement with the finding of no change in the excimer fluorescence of PI−N3C and PM−N3C.

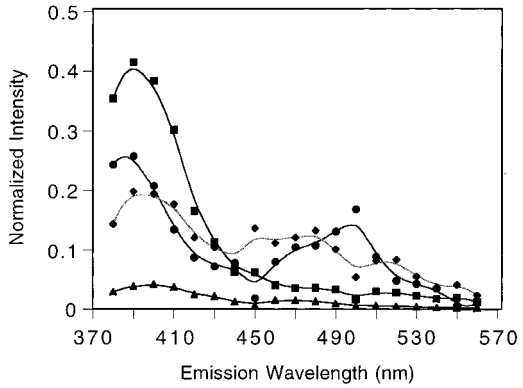

FIGURE 5: Decay-associated emission spectra of PI−N3C at 320 nm excitation wavelength. Lifetime component: (▲) 0.99 ns, (◆, light line) 4.6 ns, (●) 15 ns, (■) 45 ns.

Time-Resolved Fluorescence. The fluorescence decay of PI−N3C mutein is complex. Four lifetime components were resolved by use of time scales ≤80 ns. A fifth lifetime that was probably >100 ns appeared upon use of a 160-ns time scale. This lifetime was too long to be determined accurately in the timing range of our instrument. Fluorescence decay data were acquired on a 40-ns time scale at 10-nm intervals from 380 to 540 nm and deconvolved simultaneously, assuming that lifetimes but not amplitudes were independent of wavelength. A three-exponential fit gave lifetimes of 0.84, 4.8, and 26 ns with an unacceptable $\chi_r^2 = 4.7$. A four-exponential fit resolved a stray light component with little change in lifetime and χ_r^2. The lifetimes were 1.4, 5.3, and 28 ns; global $\chi_r^2 = 3.7$. The corresponding single curve analyses gave χ_r^2 values in the range of 1.3−1.5. A global analysis assuming five exponentials with the stray light unlinked gave lifetimes of 0.99, 4.6, 15, and 45 ns with $\chi_r^2 = 1.4$. Figure 5 plots the decay-associated emission spectra of the four lifetime components. The spectra are a bit noisy, probably reflecting correlation among the parameters of the five-exponential fit. All four components have positive amplitudes at both monomer and excimer emission wavelengths. The 0.99- and 45-ns components represent primarily the monomer band, whereas the 4.6- and 15-ns components contribute to both monomer and excimer bands. The fluorescence decay of PI−Cys at 400 nm emission wavelength was best fit by three exponentials with lifetimes of 0.8, 7.1, and 23 ns and χ_r^2 of 1.3.

Time-Resolved Anisotropy. Fluorescence anisotropy decays were collected for both pyrene-labeled N3C endonucleases on several time scales between 13 and 165 ns. Anisotropy decays were measured at 400 nm in the monomer emission band on 5×10^{-6} M PI−N3C or PM−N3C in the absence and presence of Mg^{2+} and on 8.3×10^{-7} M PI−N3C−DNA or PM−N3C−DNA complexes. The anisotropy decays of all N3C samples were best fit by a sum of two exponentials (Table 3). A three-exponential fit did not result in significant improvement in χ_r^2 values. The $r(0)$ values for the biexponential fit agreed with the values of the

Table 3: Anisotropy Decay Parameters[a]

sample	β_1	ϕ_1 (ns)	β_2	ϕ_2 (ns)	$\chi_r^{2\,b}$	$r(0)$
PI−Cys	0.18 ± 0.02	0.35 ± 0.05			1.4	0.20 ± 0.08[c]
PI−N3C	0.17 ± 0.20	20 ± 5			2.6	0.17 ± 0.02
	0.05 ± 0.02	3 ± 1	0.13 ± 0.02	60 ± 30	2.3	0.18 ± 0.04
single pyrene	0.10 ± 0.01	60 ± 20			2.5	
	0.16 ± 0.02	0.4 ± 0.1	0.097 ± 0.06	100 ± 60	2.4	0.26 ± 0.02
PI−N3C−DNA	0.165 ± 0.008	26.5 ± 0.7			2.9	0.165 ± 0.008
	0.07 ± 0.01	3.8 ± 0.7	0.12 ± 0.02	76 ± 6	2.2	0.19 ± 0.03
PI−N3C−Mg^{2+}	0.159 ± 0.005	21.5 ± 0.2			2.0	0.159 ± 0.005
	0.06 ± 0.02	2.3 ± 0.2	0.132 ± 0.004	50 ± 10	1.8	0.19 ± 0.02
PM−Cys	0.18 ± 0.03	0.34 ± 0.03			2.7	0.19 ± 0.04[c]
PM−N3C	0.178 ± 0.009	60 ± 8			2.1	0.178 ± 0.009
	0.025 ± 0.006	2 ± 1	0.17 ± 0.01	100 ± 25	1.9	0.18 ± 0.02
PM−N3C−DNA	0.175 ± 0.005	50 ± 3			2.6	0.175 ± 0.005
	0.035 ± 0.005	1.2 ± 0.2	0.161 ± 0.003	97 ± 4	1.8	0.20 ± 0.01
PM−N3C−Mg^{2+}	0.148 ± 0.002	43 ± 7			4.8	0.148 ± 0.002
	0.034 ± 0.007	0.7 ± 0.3	0.138 ± 0.003	70 ± 4	2.5	0.17 ± 0.01

[a] Emission wavelength 400 nm. Errors are standard deviations for at least three measurements. [b] Global χ_r^2 values are elevated by scattered light in the vertically polarized decay. Individual χ_r^2 values are 1.2−1.4 for magic angle decay, 1.6−1.9 for horizontally polarized decay, and 2.2−2.8 for vertically polarized decay. [c] Fundamental anisotropy r_0.

fundamental polarization r_0 of cysteine conjugate, suggesting that the observed anisotropy decay accounts for all of the probe motion. The anisotropy decay parameters of pyrene-labeled N3C endonucleases were not affected by binding of substrate and cofactor within error.

The short rotational correlation time of 0.4−3 ns represents local motion of the pyrene, while the poorly determined long rotational correlation time of 50−100 ns represents overall tumbling of the protein. The rotational correlation time for a sphere the size of *Eco*RI endonuclease in 0.6 M NaCl buffer containing 10% glycerol at 4 °C calculated from the Stokes−Einstein equation is 73 ns. The rotational correlation time for the cysteine conjugate is 350 ps (Table 3). When only one N-terminus in PI−N3C is labeled, the fraction of pyrene rings undergoing rapid internal motion estimated from the relative β values is 60%. The rotational correlation time of 400 ps is the same within error as the value for PI−Cys, consistent with free rotation of the pyrene ring about a flexible linkage. Two control experiments confirm that the 400 ps rotational correlation time is not due to free probe: (1) PI−N3C samples prepared by labeling for short times with excess reagent or for long times with limiting reagent give the same anisotropy parameters. (2) Dialysis of PI−N3C for 3 days with buffer changes every 4−6 h has no effect on the anisotropy parameters. When both N-termini are labeled, most of the probe population reports the overall protein motion. Stacking of the pyrene rings hinders the rapid internal motion, reducing the mobile pyrene fraction to 28% for PI−N3C and 14% for PM−N3C. The rotational correlation time of 1−3 ns probably involves both free rotation of the probe and segmental motion of the N-terminal region. This possibility was tested by global analysis of anisotropy data sets for PI−N3C with one pyrene and PI−N3C with two pyrenes acquired on short time scales (10−13 ns). The fit to three exponentials with lifetimes and rotational correlation times linked gives rotational correlation times of $\phi_1 = 300$ ps, $\phi_2 = 5.6$ ns, and $\phi_3 = 90$ ns with global $\chi_r^2 = 2.5$, close to the χ_r^2 values for individual biexponential fits in Table 3. Here we attribute the very short rotational correlation time to free rotation of pyrene rings and the intermediate rotational correlation time to segmental motion of the N-termini. As expected, PI−N3C with only one N-terminus labeled has a large amount of freely rotating pyrene and just a small amount of segmental motion with $\beta_1 = 0.12$, $\beta_2 = 0.02$, and $\beta_3 = 0.09$; whereas PI−N3C with both N-termini labeled has a small amount of freely rotating pyrene compared to segmental motion with $\beta_1 = 0.03$, $\beta_2 = 0.07$, and $\beta_3 = 0.13$.

DISCUSSION

Site-directed fluorescence spectroscopy is an excellent method for investigating the conformation of the N-termini of *Eco*RI endonuclease. Cysteine substitution and fluorescent labeling at Asn3 had only minor effects on binding and cleavage activity of endonuclease. This was anticipated from proteolytic deletion studies, in which deletion of residues 2−4 (residue 1 is missing in mature enzyme) has little effect in wild-type enzyme (*16*). Pyrene excimer fluorescence and chemical cross-linking offer compelling evidence for proximity of the two Cys3 in the N-termini of *Eco*RI homodimer. In wild-type endonuclease, the Cys218 residues are resistant to sulfhydryl reagents. It is unlikely that the cysteine substitution at position 3 would alter the reactivity of Cys218. In the X-ray crystal structure of *Eco*RI−DNA complex, the two Cys218 residues are 30 Å apart on opposite sides of the dimer interface with their sulfhydryl groups buried in the protein interior and α-carbons exposed on the protein surface. Intermolecular excimer formation is ruled out by constant intensity ratios of excimer to monomer emission with protein concentration. Intermolecular cross-linking is ruled out by the low protein concentrations used in the cross-linking reaction and by the drop in cross-linking efficiency with longer spacers. Binding of cognate DNA or Mg^{2+} has no apparent effect on the proximity of the N-termini, as judged by intensity ratios and chemical cross-linking.

Excimer emission in pyrene-derivatized macromolecules has been widely used to probe spatial proximity. The traditional model of excimers is based on studies in organic solvents, where pyrene does not form ground-state dimer or stacks. In organic solvents, excimer formation is a dynamic process in which excited monomer collides with ground-state monomer to form excited dimer or excimer. The excitation and emission spectra and intensity ratio do not depend on emission and excitation wavelength, and the time-

resolved fluorescence shows the classical signature of excited-state reactions: a negative amplitude in the fluorescence decay. The excimer in PI−N3C has none of these properties. Moreover, the difference in absorption spectra of cysteine and protein conjugates plus the wavelength dependence of the excitation and emission spectra and intensity ratio all point to the presence of ground-state stacks as well as unstacked pyrene in pyrene-labeled N3C. In pyrene crystals, the aromatic rings are arranged in parallel pairs and only excimer emission is observed (*33*). In protein conjugates, the pyrene rings likely adopt multiple stacked configurations, some of which may emit at the monomer or excimer wavelengths while others are nonfluorescent. The absorption spectra of PI−Cys and PM−Cys are identical. The absorption spectra of PI−N3C and PM−N3C are similar; both are much broader than the spectra of cysteine conjugate. The intensity ratio of excimer to monomer emission at 340 nm excitation wavelength is only 26% in PI−N3C, much lower in PM−N3C. A plausible interpretation of the low intensity ratios is that many of the stacked pyrenes are unable to achieve the optimal configuration for excimer emission, so that the pyrene stacks emit either at the monomer wavelength or not at all. This limitation is more severe in PM−N3C than PI−N3C, because the maleimide ring is less flexible than the iodoacetamide linkage.

Proximity of the N-termini in *Eco*RI endonuclease is supported by chemical cross-linking studies of N3C. Several cross-linking reagents linked the two subunits together through Cys3 on each polypeptide chain, giving a dimer band on SDS gels. Disulfide bond formation by DTNB was quite efficient, demonstrating that the distance between Cys3 sulfhydryls in N3C can be as short as 2.5 Å. This compares with distances of 11 and 17 Å between sulfhydryls for the excimers in PI−N3C and PM−N3C. Given the 2-fold symmetry of *Eco*RI dimer (*5*) and proximity of the N-termini, the most likely location for the N-termini is around the dimer interface.

Mobility of the N-termini was investigated by time-resolved emission anisotropy studies of pyrene-labeled N3C. Anisotropy decays indicate two rotational correlation times for stacked and unstacked pyrene in N3C in the absence and presence of DNA or Mg^{2+}. The two rotational correlation times suggest a minor mobile pyrene species moving independently of the protein and a major species rigidly attached and moving with the protein. The short rotational correlation times probably represent rotation of stacked and unstacked pyrene about the covalent linkage as well as segmental motions of the N-termini.

The 16-residue N-terminal sequence of *Eco*RI endonuclease is Ser-Asn-Lys-Lys-Gln-Ser-Asn-Arg-Leu-Thr-Glu-Gln-His-Lys-Leu (the first residue fMet is not present). Five of 16 residues are charged at neutral pH. All but the two Leu residues at positions 10 and 16 are hydrophilic. Hydrophilic residues are more likely to be on the protein surface than buried in the protein interior. A fully extended polypeptide chain of 16 amino acids is 44 Å. Molecular modeling using the Momany program in QUANTA predicts 1.5 turns of α-helix from Ser7 to Glu12. Assuming no other regular secondary structure, the predicted N-terminus would comprise 14 Å of extended chain from residues 2−6, a 90° turn of α-helix from residues 7−12, and another 11 Å of extended chain from residues 13−16. The direct distance from Ser2 to the first ordered residue in the X-ray structure, Ser17, would be 24 Å. Such an ordered structure is usually resolved in X-ray crystal structures. The fluorescence studies reported here do not support the notion of a flexible, random structure. The failure to see the N-terminal region in the X-ray structure is probably not because it is disordered, but because as a crystallographic artifact it is entangled at the crystallographic 3-fold axis. Of course, a hydrophobic probe such as pyrene undoubtedly prefers a location on the protein surface rather than in the aqueous solvent. Therefore, future studies with different probes and labeling positions are necessary to strengthen this conclusion.

*Bam*HI endonuclease has structural similarities to *Eco*RI endonuclease, although it is considerably smaller (*4*, *34*). The core structural elements of both enzymes consisting of five β-strands and two α-helices (β3−β7, α4, and α6 in *Bam*HI; β1−β5, α4, and α5 in *Eco*RI) can be superimposed with an overall root-mean-square deviation of ∼2 Å. The common core motif contains the majority of the active site, DNA cleft, and dimer interface residues. The N- and C-termini are on opposite sides of the common core motif in the two proteins, and two analogous α-helices (α2 and α7 in *Bam*HI, α6 and α1 in *Eco*RI) run in opposite directions in the two enzymes. The α7 helices at the C-termini of *Bam*HI homodimer unfold upon binding of cognate DNA (*35*). Helix α7 from one subunit folds back toward the core of the protein and α7 from the other subunit wraps DNA from the side distal to the subunit interface by binding to the minor groove of DNA. In the *Eco*RI−DNA complex, the N-terminal 16 residues just before helices α1, which are the counterparts of helices α7 in *Bam*HI, are not resolved (*6*). However, since wrapping of DNA is accomplished by the inner (residues 116−147) and outer (residues 171−199) arms of *Eco*RI endonuclease, whose counterparts are absent in *Bam*HI endonuclease, the analogous unfolding change of the N-termini of *Eco*RI endonuclease associated with specific DNA binding is unlikely to occur, even given an ordered secondary structure for the N-termini.

ACKNOWLEDGMENT

We thank Mr. Michael Kurpiewski for excellent technical assistance. We also thank an anonymous reviewer for raising an interesting question and Dr. Jay R. Knutson for helpful discussions about the possibility of depolarization due to excimer formation, which we addressed by anisotropy experiments on protein labeled with a single pyrene.

REFERENCES

1. Roberts, R. J., and Halford, S. E. (1993) in *Nucleases* (Linn, S. M., Lloyd, R. S., Roberts, R. J., Eds.) Cold Spring Harbor Laboratory Press, Cold Spring Harbor, NY.
2. Pingoud, A., and Jeltsch, A. (1997) *Eur. J. Biochem. 246*, 1−22.
3. Roberts, R. J., and Macelis, D. (1993) *Nucleic Acids Res. 21*, 3125−3137.
4. Aggarwal, A. K. (1995) *Curr. Opin. Struct. Biol. 5*, 11−19.
5. McClarin, J. A., Frederick, C. A., Wang, B.-C., Greene, P., Boyer, H. W., Grable, J., and Rosenberg, J. M. (1986) *Science 234*, 1526−1541.
6. Kim, Y., Grable, J. C., Love, R., Greene, P. J., and Rosenberg, J. M. (1990) *Science 249*, 1307−1309.

7. Rosenberg, J. M. (1991) *Curr. Opin. Struct. Biol. 1*, 104−113.
8. Lesser, D. R., Kurpiewski, M. R., and Jen-Jacobson, L. (1990) *Science 250*, 776−786.
9. Wolfes, H., Alves, J., Fliess, A., Geiger, R., and Pingoud, A. (1986) *Nucleic Acids Res. 14*, 9063−9080.
10. Wright, D. J., King, K., and Modrich, P. (1989) *J. Biol. Chem. 264*, 11816−11821.
11. King, K., Benkovic, S. J., and Modrich, P. (1989) *J. Biol. Chem. 264*, 11807−11815.
12. Grabowski, G., Maass, G., and Alves, J. (1996) *FEBS Lett. 381*, 106−110.
13. Windolph, S., and Alves, J. (1997) *Eur. J. Biochem. 244*, 134−139.
14. Heitman, J., and Model, P. (1990) *EMBO J. 9*, 3369−3378.
15. Flores, H., Osuna, J., Heitman, J., and Soberon, X. (1995) *Gene 157*, 295−301.
16. Jen-Jacobson, L., Lesser, D., and Kurpiewski, M. (1986) *Cell 45*, 619−629.
17. Förster, T. (1969) *Angew. Chem., Int. Ed. Engl. 8*, 333−343.
18. Ozawa, H. (1967) *J. Biochem. (Tokyo) 62*, 531−536.
19. Lesser, D. R., Grajkowski, A., Kurpiewski, M. R., Koziolkiewicz, M., Stec, W. J., and Jen-Jacobson, L. (1992) *J. Biol. Chem. 267*, 24810−24818.
20. Hill, T. L., and Mayhew, J. W. (1990) *J. Chromatogr. 512*, 415−431.
21. Cheng, S.-C., Kim, R., King, K., Kim, S.-H., and Modrich, P. (1984) *J. Biol. Chem. 259*, 11571−11575.
22. Greene, P. J., Heyneker, H. L., Boliver, F., Rodriguez, R. L., Beltach, M. C., Covarrubias, A. A., Backman, K., Russel, D. J., Tait, R., and Boyer, H. W. (1978) *Nucleic Acids Res. 5*, 2373−2380.
23. Haugland, R. P. (1996) *Handbook of Fluorescent Probes and Research Chemicals*, 6th ed., Molecular Probes, Inc., Eugene, OR.
24. Riggs, A. D., Suzuki, H., and Bourgeois, S. (1970) *J. Mol. Biol. 48*, 67−83.
25. Riggs, A. D., Bourgeois, S., and Cohn, M. (1970) *J. Mol. Biol. 53*, 401−417.
26. Jen-Jacobson, L., Kurpiewski, M., Lesser, D., Grable, J., Boyer, H. W., Rosenberg, J. M., and Greene, P. J. (1983) *J. Biol. Chem. 258*, 14638−14646.
27. Beechem, J. M. (1989) *Chem. Phys. Lipids 50*, 237−251.
28. Modrich, P., and Zabel, D. (1976) *J. Biol. Chem. 251*, 5866−5874.
29. Rawat, M., and Maroney, J. V. (1991) *J. Biol. Chem. 266*, 9719−9723.
30. Ishii, Y., and Lehrer, S. S. (1989) in *Fluorescent Biomolecules* (Jameson, D. M., Reinhart, G. D., Eds.) Vol. 51, pp 423−425, Plenum, New York.
31. Lehrer, S. S. (1997) *Methods Enzymol. 278*, 286−295.
32. Reichert, A., Heintz, D., Echner, H., Voelter, W., and Faulstich, H. (1996) *J. Biol. Chem. 271*, 1301−1308.
33. Birks, J. B. (1975) *Rep. Prog. Phys. 38*, 903−974.
34. Newman, M., Strzelecka, T., Dorner, L. F., Schildkraut, I., and Aggarwal, A. K. (1994) *Nature 368*, 660−664.
35. Newman, M., Strzelecka, T., Dorner, L., Schildkraut, I., and Aggarwal, A. (1995) *Science 269*, 656−663.

BI980557F